Seventh International Conference on CFD in the Minerals and Process Industries
CSIRO, Melbourne, Australia
9-11 December 2009

MODELLING THE FLUID DYNAMICS AND THE GROWTH KINETICS OF FLUIDIZED BED SPRAY GRANULATION

Zhen LI[1], Matthias KIND[1] and Gerald GRUENEWALD[2]

[1] Institute of Thermal Process Engineering, University of Karlsruhe, Germany
[2] BASF SE, Ludwighafen, Germany

ABSTRACT

Fluidized bed spray granulation is used to produce porous granular particles from suspensions and solutions. Experimental investigations and modelling of the mechanisms revealed that the fluid dynamics in the granulator, in particular in the jet flow, which causes the particle movement as well as drop propagation and deposition on the particles, play a crucial role. Therefore, in this work the "Two Fluid Model" (TFM) is used to simulate the fluid dynamics in the fluidized bed and the jet. The simulated results were validated by measuring the particle velocity with Laser Doppler Velocimetry (LDV). The growth kinetics can be obtained by modelling the growth mechanisms like droplet deposition, dust integration and particle drying with the "User-defined Functions". The population balance approach is used to describe the transient granulation process and the particle growth. The Quadrature Method of Moments (QMOM) is adopted as a solution method for the population balance in this work. The coupled simulation of CFD and population balances allows a complete description of the process.

NOMENCLATURE

C_D	drag coefficient
d	diameter
e_{ss}	restitution coefficient
g	gravitational acceleration
$g_{0,ss}$	radial distribution function
G_L	growth rate
h	adhesion probability
m_k	kth moment
p	pressure
$\vec{v}$	velocity
α	volume fraction
φ	impingement efficiency
η	deposition efficiency
λ_s	bulk viscosity
μ	dynamic viscosity
Θ_s	granular temperature
ρ	density
σ	surface tension
$\bar{\bar{\tau}}$	strain tensor

Dimensionless number

Oh	Ohnesorge number
Re	Reynolds number
St	Stokes number
We	Weber number

INTRODUCTION

In this process the suspension is atomized by a nozzle and injected into a fluidized bed with the same material. The droplets are deposited on the surface of the particles and form a film which is dried with the hot fluidization air to build a solid layer. Due to the high velocity of the jet flow the particles circulate between a near-nozzle zone, where the particles are humidified, a freeboard above the jet flow and the remaining fluidized bed, where the particles are dried. Several mechanisms are important for this process. Seed particles can be formed from small dust particles and droplets, then grow to become nuclei, which remain in the fluidized bed and grow to particles of desired product size range. Surely negative growth due to breakage and attrition can also take place. On account of the rudimentary knowledge of the interaction of the single mechanisms, design of such a process is based primarily on experience and know-how. Hence, the research in this area is aimed at the understanding of the process. The coupled simulation of CFD and population balance enables us to find suitable process parameters and to predict the particle properties, like particle size distribution.

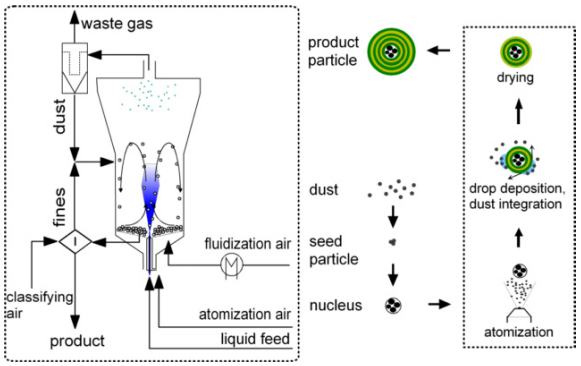

Figure 1: Schematic diagram of plant geometry.

MATHEMATICAL MODEL

In the "Two Fluid model" the fluid phase and the solid phases are treated as interpenetrating continua by incorporating the concept of phase volume fractions α_q.

The summation of the volume fractions must be 1.

$$\sum_{q=1}^{q=n} \alpha_q = 1 \qquad (1)$$

The conservation laws of mass and momentum must be solved for every phase to account for the interphase forces.

Conservation of Mass

The continuity equation for each of the phases is:

$$\frac{\partial}{\partial t}\left(\alpha_q \rho_q\right)+\nabla\cdot\left(\alpha_q \rho_q \vec{v}_q\right)=S_q \tag{2}$$

Conservation of Momentum

The momentum balance for phase q yields

$$\frac{\partial}{\partial t}\left(\alpha_q \rho_q \vec{v}_q\right)+\nabla\cdot\left(\alpha_q \rho_q \vec{v}_q \vec{v}_q\right)=-\alpha_q \nabla\cdot P + \nabla\cdot\bar{\bar{\tau}}+\alpha_q \rho_q g+\sum K_{pq}\left(\vec{v}_p-\vec{v}_q\right)+\left(\vec{F}_q+\vec{F}_{lift,q}+\vec{F}_{vm,q}\right) \tag{3}$$

where $\vec{F}_q$ is the external body force, $\vec{F}_{lift,q}$ is the lift force, $\vec{F}_{vm,q}$ is the virtual mass force. In this investigation the lift force and virtual mass force are neglected.

$\bar{\bar{\tau}}$ is the stress strain tensor of the q[th] phase

$$\bar{\bar{\tau}}=\alpha_q \mu_q\left(\nabla\vec{v}_q+\nabla\vec{v}_q^{\,T}\right)+\alpha_q\left(\lambda_q-\frac{2}{3}\mu_q\right)\nabla\cdot\vec{v}_q\bar{\bar{\mathbf{I}}} \tag{4}$$

$\bar{\bar{\mathbf{I}}}$ is the unit tensor. μ_q and λ_q are the shear and bulk viscosity of the solid phase q and they are discussed in the next section on the kinetic theory of granular flow. The moment transfer coefficient was calculated with Gidaspow's model.

$$K_{g,s,Ergun}=150\frac{\alpha_s^2\mu_g}{\alpha_g d_p^2}+1.75\frac{\alpha_s\rho_g}{d_p}\left|\vec{v}_g-\vec{v}_s\right|,\ \alpha_g<0.8 \tag{5}$$

$$K_{g,s,Wen-Yu}=\frac{3}{4}C_D\frac{\alpha_s\rho_g}{d_p}\left|\vec{v}_g-\vec{v}_s\right|\alpha_g^{-2.65},\qquad \alpha_g\geq 0.8 \tag{6}$$

To avoid the discontinuity of the two equations, Gidaspow introduced a switch function that gives a rapid transition from one regime to the other.

$$\varphi_{g,s}=\frac{\arctan\left[150\times 1.75(0.2-\alpha_s)\right]}{\pi}+0.5$$

Thus, the moment transfer coefficient can be written as

$$K_{g,s}=\left(1-\varphi_{g,s}\right)K_{g,s,Ergun}+\varphi_{g,s}K_{g,s,Wen-Yu} \tag{7}$$

The drag coefficient depends on the Reynolds number and is expressed as

$$C_D=\frac{24}{\mathrm{Re}_s}\left[1+0.15\left(\mathrm{Re}_s\right)^{0.687}\right],\qquad \mathrm{Re}_s<1000$$

$$C_D=0.44,\qquad \mathrm{Re}_s\geq 1000 \tag{8}$$

Kinetic Theory of Granular Flow

The granular temperature for the solid phase Θ_s is proportional to the kinetic energy of the random motion of the particles. The transport equation derived from kinetic theory takes the form

$$\frac{3}{2}\left[\frac{\partial}{\partial t}\left(\rho_s\alpha_s\Theta_s\right)+\nabla\cdot\left(\rho_s\alpha_s\vec{v}_s\Theta_s\right)\right]=\left(-P_s\bar{\bar{\mathbf{I}}}+\bar{\bar{\tau}}_s\right):\nabla\vec{v}_s-\nabla\cdot\left(k_s\nabla\Theta_s\right)-\gamma\cdot\Theta_s+\phi_{g,s} \tag{9}$$

where $\left(-P_s\bar{\bar{\mathbf{I}}}+\bar{\bar{\tau}}_s\right):\nabla\vec{v}_s$ is the generation of energy by the solids stress tensor, $k_s\nabla\Theta_s$ describes the diffusion of energy, the diffusion coefficient k_s is expressed as

$$k_s=\frac{150\rho_s d_s\sqrt{(\Theta\pi)}}{384(1+e_{ss})g_{0,ss}}\left[1+\frac{6}{5}\alpha_s g_{0,ss}(1+e_{ss})\right]^2+2\rho_s\alpha_s^2 d_s(1+e_{ss})g_{0,ss}\sqrt{\frac{\Theta_s}{\pi}} \tag{10}$$

and $\gamma\cdot\Theta_s$ is the collisional dissipation of energy.

$$\gamma\cdot\Theta_s=\frac{12\left(1-e_{ss}^2\right)g_{0,ss}}{d_p\sqrt{\pi}}\rho_s\alpha_s^2\Theta_s^{3/2} \tag{11}$$

The restitution coefficient was assumed to be 0.9. The radial distribution function was calculated by the Lun's model:

$$g_{0,ss}=\left[1-\left(\frac{\alpha_s}{\alpha_{s,\max}}\right)^{1/3}\right]^{-1} \tag{12}$$

The solids stress tensor contains shear and bulk viscosities arising from particle momentum exchange due to translation and collision. A frictional component of viscosity can also be included to account for the viscous-plastic transition that occurs when particles of a solid phase reach the maximum solid volume fraction. The collisional and kinetic parts, and the optional frictional part, are added to obtain the solids shear viscosity:

$$\mu_s=\mu_{s,col}+\mu_{s,kin}+\mu_{s,fric} \tag{13}$$

The collisional part of the shear viscosity is modelled as

$$\mu_{s,col}=\frac{4}{5}\alpha_s\rho_s d_p g_{0,ss}(1+e_{ss})\left(\frac{\Theta_s}{\pi}\right)^{1/2} \tag{14}$$

The following optional expression from Gidaspow et al. is for the kinetic part

$$\mu_{s,kin}=\frac{10\rho_s d_p\sqrt{\Theta_s\pi}}{96\alpha_s(1+e_{ss})g_{0,ss}}\left[1+\frac{4}{5}g_{0,ss}\alpha_s(1+e_{ss})\right]^2 \tag{15}$$

The solids bulk viscosity accounts for the resistance of the granular particles to compression and expansion. According to Lun et al., this property can be described by:

$$\lambda_s=\frac{4}{3}\alpha_s^2\rho_s d_p g_{0,ss}(1+e_{ss})\sqrt{\frac{\Theta_s}{\pi}} \tag{16}$$

Droplet Deposition

Following Loeffler (1988), the deposition efficiency η can be split into two parts, the impingement efficiency φ and the adhesion probability h. The impingement efficiency describes the ratio of the number of droplets which actually collide with the particle to the number of droplets in the total projection area of the particle. It can be expressed as a function of the Stokes number and the Reynolds number.

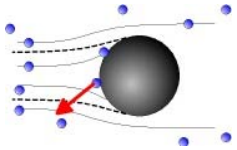

Figure 2: Droplet deposition

The deposition efficiency of droplets on one particle is:

$$\eta=\varphi\cdot h \tag{17}$$

$$\varphi=\left(\frac{St}{St+b}\right)^a \tag{18}$$

where a and b are empirical parameters, which are constant in different intervals of the Reynolds number (Appendix A). The adhesion probability can be estimated with the approach of Mundo (1995). A critical collision velocity depending on material properties can be calculated. If a droplet has a velocity lower than the critical velocity, it will spread on the surface of the granules. Above the critical velocity, it will be atomized or rebound. The critical velocity is described as a function of the Ohnesorge number Oh.

$$v_{krit} = \frac{57{,}7^{0,8}\,\mu_{tr}}{Oh^{0,8} d_{tr} \rho_{tr}} \tag{19}$$

The Ohnesorge number is defined as

$$Oh = \frac{\mu_{tr}}{\sqrt{\rho_{tr}\sigma_{tr} d_{tr}}} = \frac{\sqrt{We}}{\mathrm{Re}} \tag{20}$$

where μ_{tr} and σ_{tr} are the viscosity and the surface tension of the droplets. Due to geometrical aspects, the adhesion probability can be calculated with the projected area of the granule surface (Zank 2001):

$$h = \left(\frac{v_{krit}}{v_{rel}}\right)^2 \tag{21}$$

The droplet deposition in a packed bed can be calculated as below

$$\frac{dN_{tr}}{N_{tr}} = 1.5 \cdot \eta \frac{1}{d_p} \frac{\alpha_p}{\alpha_g} dh \tag{22}$$

In order to obtain a discretized form of the equation, the differential height dh is linked to an equivalent cell size with the residual time in the corresponding cell. The deposition efficiency in a cell can then be calculated by integration of the equation above.

$$\frac{\Delta N_{tr}}{N_{tr}} = 1 - \exp(-1.5 \cdot \eta \frac{1}{d_p} \frac{v_{rel}\alpha_p}{\alpha_g} \Delta t_v) \tag{23}$$

Population Balance approach

The simplest experimental test case is a semi-batch granulation, where the granules grow only due to droplet deposition. The number of granules (the 0. moment) is conserved. In the Two Fluid Model, the droplet deposition is only calculated for a monodisperse system, therefore the particle growth rate is not a function of particle size, but of time. The growth rate can be calculated as the solid volume in the deposited droplets divided by the total surface of particles in the granulator.

$$G_L(t) = \frac{\dot{V}_s D_{total}(t)}{N_P\left(m_2(t)/m_0(t)\right)} \tag{24}$$

where N_p is the particle number and D the total deposition efficiency over all cells. The population balance is solved in this work with the Quadrature Method of Moments (QMOM). The transport equations of moments are as follows:

$$\frac{dm_k}{dt} = Growth_k \tag{25}$$

$$Growth_k = \sum_{i=1}^{N} k w_i L_i^k G_L(t) \tag{26}$$

The particle size distribution was reconstructed from the first N moments with the statistically most probable distribution (Pope, 1979). The PSD can be expressed as

$$n(L) = \frac{dN_P}{dL} = \exp\left(\sum_{i=0}^{N-1} A_i L^i\right) \tag{27}$$

The equation for the kth moment is written as:

$$m_k = \int_0^\infty L^k \exp\left(\sum_{i=0}^{N-1} A_i L^i\right) dL \tag{28}$$

For given N moments, the coefficients A_i can be found to reconstruct the PSD.

MESH AND BOUNDARY CONDITIONS

For the two phase system a 2D axis-symmetric model was adopted. Due to the nozzle geometry, the swirl flow at the orifice can not be neglected. In order to get the boundary conditions for the 2D calculations at the orifice, a complete 3D model was created. With this model the fluid dynamics of the air in the nozzle and the orifice was simulated.

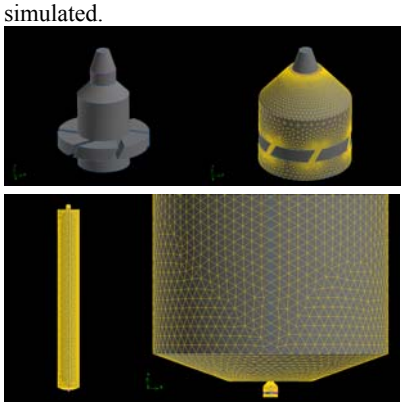

Figure 3: 3D grid of nozzle and granulator

The nozzle configuration is shown in Figure 3. There are 6 skewed slits in the nozzle, which cause a high tangential velocity of 120 m/s at the orifice. This stabilizes the jet and enhances the atomizing effect. The measurement of the velocity close to the orifice is difficult to realize. With the help of the 3D simulation the three components of the air velocity at the orifice can be obtained and can be used as the boundary conditions for the 2D simulations. The nozzle was meshed separately since it is very small compared to the whole apparatus. In the 2D grid the nozzle was created with the simplification that the nozzle is just treated as a jet hole with the boundary conditions mentioned above. The detailed nozzle geometry was neglected. This is based on the assumption, that in a certain distance from the orifice, the flow is independent of nozzle itself as long as the boundary conditions are correct. A pave mesh method was used to mesh the face in order to reduce the number of cells. The simulations of the same pave mesh with significantly more cells and of the mapped mesh (Appendix B) yield similar results. The mesh was finer at the orifice and gradually coarser in the free board.

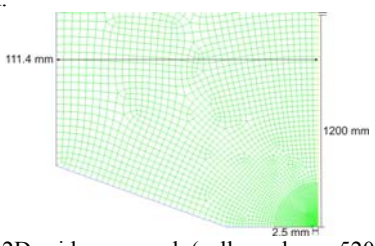

Figure 4: 2D grid pave mesh (cell number = 5200)

The boundary conditions and models to describe the granular phase are listed in Table 1 and Table 2

boundary	2D	boundary conditions
nozzle air	Mass-flow inlet	12 kg/h 30°C
fluidizing air	Mass-flow inlet	105 kg/h, 100°C
outlet	Pressure outlet	
side wall	Wall	adiabatic

Table 1: boundary conditions

parameter	model and constant
particle diameter	650 μm
particle density	1700 kg/m^3
bulk viscosity	Lun et al.
granular viscosity	Gidaspow
radial distribution	Lun et al.
solid pressure	Lun et al.
drag force	Gidaspow
packing limit	0.63
restitution coefficient	0.9

Table 2: parameters and models to describe the granular phase

EXPERIMENTS

A Laser Doppler Velocimeter (LDV) was used to measure the velocity of the particles in the jet flow. The particles were classified by sieving with mesh sizes of 630 and 700 µm. The Sauter mean diameter of the particles was 650 µm. The bed mass was 1000g. Figure 5 shows the experimental configuration.

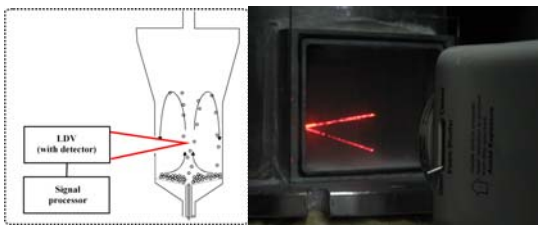

Figure 5: Experimental configuration

RESULTS

The simulations were always performed twice with the same mesh. One simulation was carried out based on the assumption, that the energy of the particles dissipates locally and the granular temperature therefore could be calculated analytically. This simulation can be used as the initial condition for the second simulation with the transport equation for granular temperature. During all the simulations, the particle velocities oscillated due to unsteady behaviour, so that the velocity at each point had to be averaged. The Reynolds Stress Model was adopted to model the turbulence in the granulator. The simulated and experimental results of the vertical particle velocity at a distance of 70 mm above the orifice are shown in Figure 6. The maximum vertical particle velocities in the middle of the jet agree well with the measured values in the case where the transport equation of granular temperature was not solved, but the width of the jet is smaller than the measured. The results of the simulation with considering the granular temperature equation agree better with the measurement with respect to jet width, but the maximum velocities in the middle of the jet flow is underestimated. However the deviation between measurement and simulation is always smaller than 20%.

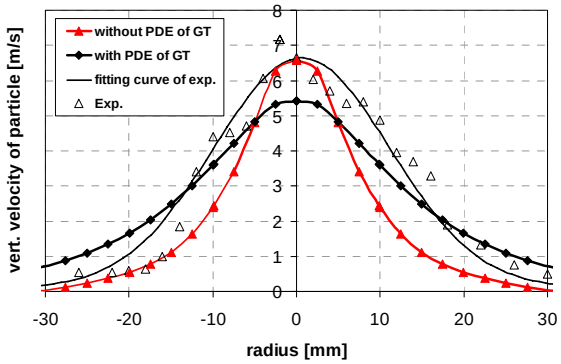

Figure 6: Vertical particle velocities from simulations and experiment (70mm above nozzle orifice)

The differences between these two calculations can be seen clearly from the velocity contour plots.

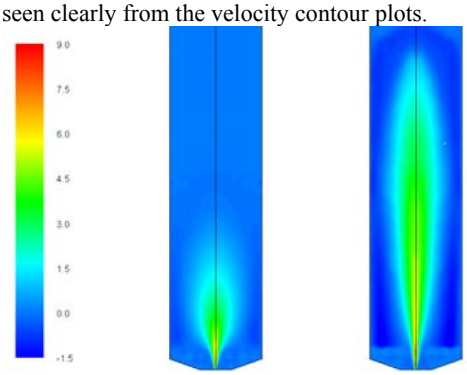

Figure 7: Velocity contours with and without solving granular temperature (m/s)

The CPU times of the simulations with different cell numbers per 10 seconds process time are listed below.

Cell number	CPU time [h]
5200	46
23000	74
93000	488

Table 3: CPU-times of simulations with different cell number (CPU: 3GHz Pentium)

Actually, due to its complexity, the simulation with 93000 cells was only calculated for 2 seconds on this computer.

It was simulated in parallel with 4 nodes (1.5 GHz per node) in a HP xc6000 cluster. It took 251 hours for 10s of process time.
For the calculation of the droplet deposition we used the simplified approach that the granular temperature is not transported and can be calculated analytically.

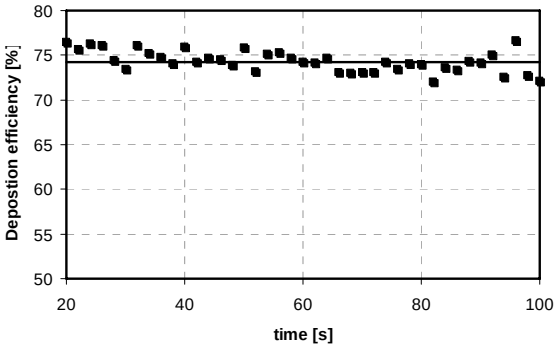

Figure 8: Total deposition efficiency in the granulator (m=1000g)

The deposition efficiencies for each simulation run oscillate a bit over time because of the unsteady calculation of the fluidized bed. Therefore, the deposition efficiencies should also be averaged (Appendix C). The deposition efficiencies of three different bed masses are listed in Table 4.

Bed Mass [g]	Diameter d_{30} [µm]	Deposition efficiency [%]
600	363	53.6
1000	430	74.2
1400	481	86.3

Table 4: Deposition efficiencies at different bed masses

The relationship of the deposition efficiency and the bed mass can be fitted as a curve. This curve can be used to calculate the growth rate for the population balance. The population balance was solved with the QMOM method.

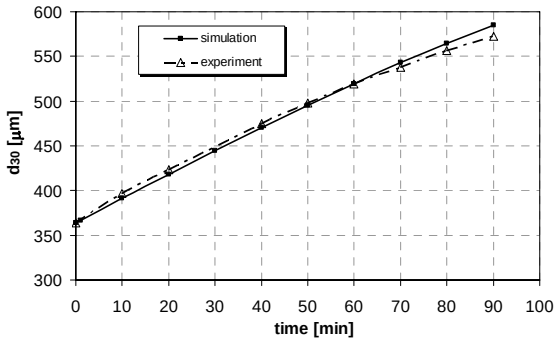

Figure 9: Development of the particle diameter over time.

Figure 9 shows the growth of the particle diameter over time. It can be seen that this method predicts the evolution of the particle diameter very well. Figure 10 shows the particle size distributions during the granulation, which were reconstructed from the moments with the method mentioned above. We assumed that the growth rate is not a function of particle size. Therefore, the shape of the PSD is preserved, whereas the measured PSD becomes lower and wider during the experiment. This means that the growth rate depends on the particle size. The large particles grow faster than the small ones. This is due to the relationship between particle size and residence time in the jet. The large particles stay in the jet flow for a longer time due to their inertia and therefore more droplets are deposited on them.

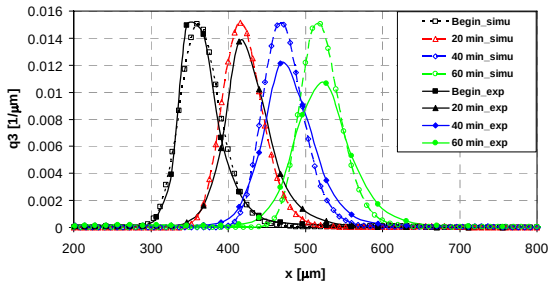

Figure 10: PSD (q_3) simulation and experiments

CONCLUSION AND OUTLOOKS

The fluid dynamics in a fluidized bed spray granulator was simulated with the "Two Fluid Model". The simulation results agree with the measured data with a deviation of less than 20%. The model is sensitive to the calculation of the granular temperature. When taking the transport equation of granular temperature into account, the particle velocity is slightly underestimated. The calculation with an analytical calculation of the granular temperature shows a good agreement with the experiment for the maximum particle velocity in the middle of the jet flow, but the jet flow was not as wide as the measured one. Including the model for the droplet deposition the evolution of the particle diameter can be well estimated. The calculated PSD preserves its shapes as a result of the assumption that the particle growth rate doesn't depend on the particle size, while the experimental PSD becomes wider. This indicates the necessity to simulate the fluid dynamics of the polydisperse system in order to obtain the growth kinetics. A "DQMOM" like method could be used to obtain the dependency of growth rate on particle size. The fluid dynamics can be simulated in a fluidized bed with three or four solid phases. The diameter and volume fraction of each phase can be calculated with the product difference method from an initial PSD. Then the growth kinetics can be obtained by calculating the droplet deposition for a few seconds with CFD. Typically the dynamics of spray granulation process is slow. Therefore, it can be assumed that the fluid dynamics does not change a lot within a few minutes, so that the population balance can be solved with regular updates of the fluid dynamics in certain time intervals. This multiscale approach may be an efficient way for a simulation of the whole granulation process.

REFERENCES

CHAPMAN, S. and COWLING, T.G. (1970), "The mathematical Theroy of Non-Uniform Gases", Academic Press, New York

DESJARDINS, O., FOX, R.O. and Villedieu, P. (2008), "A quadrature-based moment method for dilute fluid-particle flows", *Journal of Computational Physics*, 227, 2514-2539

DING, J.M and, Lu, H.L. (2004), "Numerical study of gas–solid flow in a precalciner using kinetic theory of

granular flow", *Chemical Engineering Journal*, 102, 151-160.

Du, W, BAO, X.J. (2006), "Computational Fluid Dynamics (CFD) modeling of spouted bed: Assessment of drag coefficient correlations", *Chemical Engineering Sci.*, 61, 1401-1420.

FAN, R, MARCHISIO, D.L and FOX, R.O. (2004), "Application of the Direct Quadrature Method of moments to polydisperse gas–solid fluidized beds", *Elsevier Sci.*

FAN, R, FOX, R.O. (2007), "Segregation in polydisperse fluidized beds: Validation of a multi-fluid model", *Chemical Engineering Sci.*, 63, 272-285.

GERA, D, SYAMLAL, M. and O'BRIEN, T.G. (2004), "Hydrodynamics of particle segregation in fluidized beds", *International Journal of Multiphase Flow* , 30, 419-428.

GIDASPOW, D. (1994), "Multiphase Flow and Fluidization, Continuum and Kinetic Theory Descriptions", Academic Press, New York

LAUDER, B.E. and REECE, G.J., (1974), "Progress in the development of a Reynolds-stress turbulence closure", *J. Fluid Mech.*, 68, 573-566.

LOEFFLER.F (1988), "Staubabscheiden", Thieme Verlag, Stuttgart and New York

MARCHISIO, D.L, FOX, R.O., VIGIL, R.D., and BARRESI, A.A. (2003), "Quadrature Method of Moments for Population-Balance Equations", *AIChE Journal*, 49, No.5.

MARCHISIO, D.L and FOX, R.O. (2005), "Solution of population balance equation using the direct quadrature method of moments", *Aerosol Sci.*, 36, 43-47

McGRAW, R, (1997), "Properties and evolution of aerosols with size distributions having identical moments", *J. Aerosol Sci.*, 29, 761-772.

MUNDO, C, SOMMERFELD, M. and TROPEA, C. (1995), "Droplet-Wall Collisions: experiments studies of the deformation and breakup process", *International Journal of Multiphase Flow*, 21, 151-173.

PANAO, M.R.O. and MOREIRA, A.L.N, (2004), "Experimental study of the flow regimes resulting from the impact of an intermittent gasoline spray", *Experiments in Fluids*, 37, 834-855.

POPE. S.B., (1979), "Probablity Distrubutions of Scalars in Turbulent Shear Flow", *Turbulent Shear Flows*, 2, 7-16.

RANDOLPH, A.D. and LARSON, M.A. (1971), "Theory of particulate Processes", Academic Press, New York and London

SYAMLAL, M., ROGERS, W. and O'BRIEN, T.J. (1993), "MFIX Documentation Numerical Technique", Department of Energy, Morgantown, WV, USA

ZANK, J., KIND, M., and SCHLUENDER, E. U., (2001) "Particle Growth and droplet deposition in fluidised bed granulation", *Powder Technology*, 120, 76-81.

APPENDIX A

Re	Re < 1	1 - 30	30 - 50	50 - 90	Re > 90
a	0.65	1.24	1.03	1.84	2
b	3.7	1.95	2.07	0.506	0.25

Table 5: constants for modelling the impingement efficiency

APPENDIX B

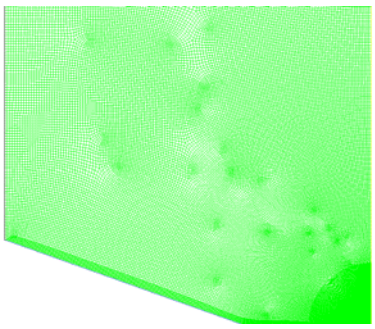

Figure 11: 2D grid pave mesh (cell number = 93000)

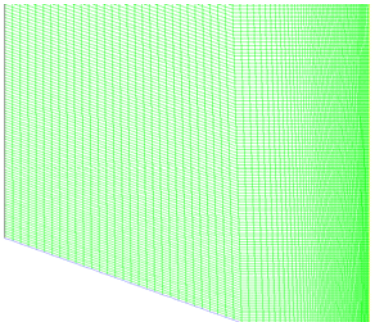

Figure 12: 2D grid mapped mesh (cell number = 44000)

APPENDIX C

The simulated total deposition efficiencies for a bed mass of 600g and 1400g are shown below.

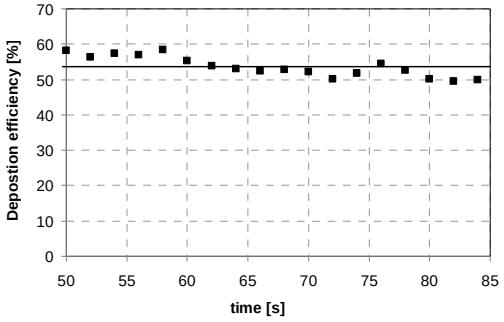

Figure 13: entire deposition efficiency in granulator (m=600g)

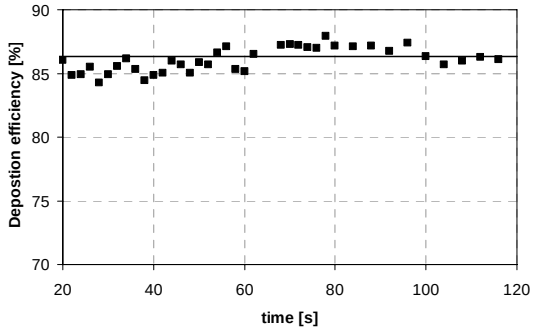

Figure 14: entire deposition efficiency in granulator (m=1400g)